

Electronic Structure and Transport Properties of Superlattices: $\text{La}_{(1-X)}\text{Sr}_X\text{TiO}_3$ ($X = 0, 0.20, 0.80, 1$)

R. K. Rai, G. C. Kaphle, R. B. Ray, O. P. Niraula

Journal of Nepal Physical Society

Volume 6, Issue 2, December 2020

ISSN: 2392-473X (Print), 2738-9537 (Online)

Editors:

Dr. Binod Adhikari

Dr. Bhawani Joshi

Dr. Manoj Kumar Yadav

Dr. Krishna Rai

Dr. Rajendra Prasad Adhikari

Mr. Kiran Pudasainee

JNPS, 6 (2), 134-148 (2020)

DOI: <http://doi.org/10.3126/jnphysoc.v6i2.34869>

Published by:

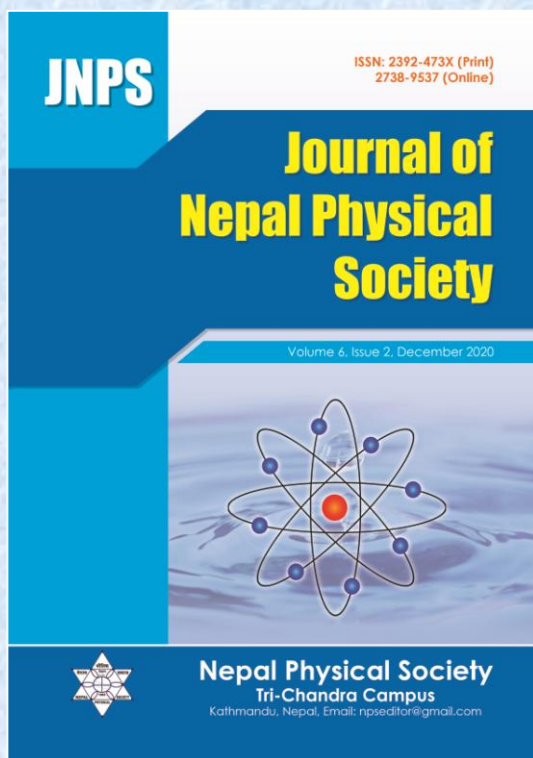
Nepal Physical Society

P.O. Box: 2934

Tri-Chandra Campus

Kathmandu, Nepal

Email: npseditor@gmail.com





Electronic Structure and Transport Properties of Superlattices: $\text{La}_{(1-x)}\text{Sr}_x\text{TiO}_3$ ($x = 0, 0.20, 0.80, 1$)

R. K. Rai^{1,2}, G. C. Kaphle^{1,*}, R. B. Ray^{1,3}, O. P. Niraula¹

¹Central Department of Physics, Kirtipur Campus, Tribhuvan University, Nepal

²Patan Multiple Campus, Lalitpur, Tribhuvan University, Nepal

³Amrit Campus, Tribhuvan University, Kathmandu, Nepal

*Corresponding Email: gck223@gmail.com

Received: 21 October, 2020; Revised: 24 November, 2020; Accepted: 28 December, 2020

Abstract

The conventional density functional theory (DFT) and dynamical mean field theory (DMFT) is used to study the structural, electronic and the Mott-Hubbard metal-insulator phase transition of the pristine and superstructures, $\text{La}_{(1-x)}\text{Sr}_x\text{TiO}_3$ ($x = 0, 0.20, 0.80, 1$). The electrical and thermal conductivities, Seebeck coefficient, Figure of merit are calculated using the BoltzTraP codes. The present study reveals that the direct band gap of 2.20 eV and indirect band gap ~ 2.0 eV at the Γ point in the Brillouin zone of SrTiO_3 is upgraded to 3.423eV by using modified Beck-Johnson (mBJ) interaction potential. The metal-insulator transition (MIT) of LaTiO_3 and the superlattice $\text{La}_{(1-x)}\text{Sr}_x\text{TiO}_3$ have been investigated by using conventional density functional theory (DFT) and dynamical mean field theory (DMFT). The Mott-Hubbard metal-insulator transitions for pristine LaTiO_3 for a Coulombian parameter, $U = 2.5$ eV and the thermodynamic parameter $\beta = 6$ (eV)⁻¹ are consistent with the experimental results. A typical set of these correlation parameters for MIT $\text{La}_{0.20}\text{Sr}_{0.80}\text{TiO}_3$ and $\text{La}_{0.80}\text{Sr}_{0.20}\text{TiO}_3$ systems are found to be $U = 3.5$ eV and $\beta = 10$ (eV)⁻¹ and $U = 3.2$ eV and $\beta = 10$ (eV)⁻¹ respectively. The characteristic sharp quasi-particle peak for a sample of $\text{La}_{0.80}\text{Sr}_{0.20}\text{TiO}_3$ superlattice systems is obtained correlation parameter $U = 3.0$ eV and $\beta = 6$ (eV)⁻¹. A thermoelectric phase transition is observed for Seebeck Coefficient at temperature 300 K at near chemical potential, $\mu = 1$ eV of SrTiO_3 . The corresponding figure of merit (ZT) with chemical potential (μ) appears to be unity at near $\mu = 1$ eV.

Keywords: DFT, DMFT, MIT, Superlattice, TMOs.

1. INTRODUCTION

The complex transition metal oxides (TMOs) are the promising smart materials for the scientific and technological innovations as well as theoretical investigation of material world. The TMOs are complex strongly correlated materials with various degrees of freedom (dof), such as charge, spin, orbital, valley and lattice interactions. The heterostructures and nanostructures of such compounds have exotic and novel properties highly useful for Mottronics applications [1, 2].

In general, these materials are found in a simple cubic perovskite ABO_3 type structures, where the A and B cations are arranged on a simple cubic lattice, and the O anions lie on the face centers

nearest to the cations (B = transition metals) as shown in Fig. 1.

The cations (A = earlier transition metals or rare earths) are at the centers of the oxygen, O octahedral, while the A cations lie at the larger 12-fold coordinated sites [3-6]. The bonding between La and TiO_2 is mainly ionic, and the TiO_2 entity is bound covalently in the LaTiO_3 system.

The density functional theory (DFT) along with the dynamical mean field theory (DMFT) is employed for figuring out the realistic electronic structure of strongly correlated system. The spectral density of distribution (spectral function) is obtained using the maximum entropy model for the La-atom substituted on Sr-site $\text{La}_{(1-x)}\text{Sr}_x\text{TiO}_3$ supercell have

been studied using various impurity solvers including quantum Monte Carlo (QMC) [7].

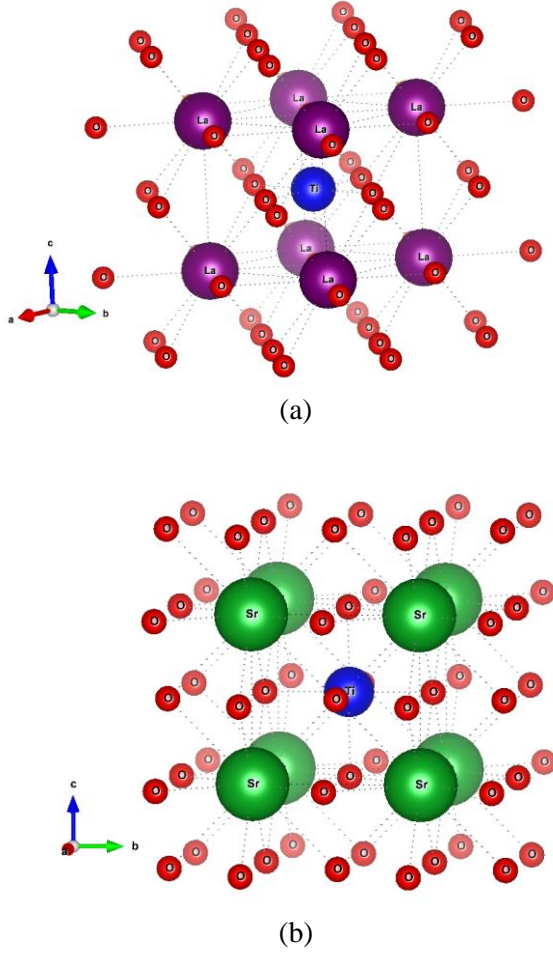


Fig. 1: (color online) The crystal structures of cubic phase of pristine (a) LaTiO_3 and (b) SrTiO_3 systems.

The strong electron correlation and other anomalous electronic properties in the metallic phase transition (MIT) are of great interest. The Mott transition in $\text{La}_{(1-x)}\text{Sr}_x\text{TiO}_3$ system is studied experimentally employing filling control method, through the appropriate doping of the holes or electrons to the system and band control method through the site substitution of Sr-ion with La-ion to the system [4,8-10].

The transition metal oxides have narrow conduction bands due to weak orbital overlap, which leads to localized electrons with low carrier mobilities. Transition metal oxides have recently been considered as thermoelectric (TE) materials that can operate at high temperature and they have their transport properties with high Seebeck coefficients (S) and low thermal conductivity (K). We have

computed the thermal conductivity K , electrical conductivity (σ/τ), Seebeck coefficients (S), and Figure of merit (ZT) etc. for the SrTiO_3 and LaTiO_3 [11, 12].

The Mottness (the resistive switching) behaviours of TMOs are highly applicable for designing novel devices, including sensing, signal conversion, non-volatile memory, artificial neurons and so on. Those oxides devices have far more better over the conventional semiconductor devices in terms of efficiency, durability, additional functionality and future downsizing to the nanoscale structures [13, 14].

2. METHODOLOGY AND COMPUTATIONAL DETAILS

2.1 Theoretical Backgrounds:

The electronic structure and transport properties of Mott-insulator LaTiO_3 and band-insulator SrTiO_3 and their superlattices systems have been investigated by using density functional theory (DFT) based quantum mechanical approach [15-17].

The optimized cubic phase of SrTiO_3 and LaTiO_3 are taken for the GGA, GGA+U+J, SOC and DOS calculations by solving self consistent Kohn-Sham equation for the many-body system as given by,

$$\left[-\frac{\hbar^2}{2m} \nabla^2 + v_{\text{eff}}(\mathbf{r}) \right] \Psi_i = \epsilon_i \Psi_i \quad (1)$$

Where the effective Kohn-Sham potential is expressed as,

$$v_{\text{eff}}(\mathbf{r}) = v(\mathbf{r}) + \int \frac{[n_e(\mathbf{r}')]^2}{|\mathbf{r}-\mathbf{r}'|} d\mathbf{r}' + v_{\text{xc}}(\mathbf{r}) \quad (2)$$

And, $v_{\text{xc}}(\mathbf{r}) = \frac{\delta E[n_e(\mathbf{r})]}{\delta n_e(\mathbf{r})}$ is the exchange

correlation potential with the probability density as,

$$n_e(\mathbf{r}) = \sum_{i=1}^N |\Psi_i(\mathbf{r})|^2$$

The electronic structure and other properties of these materials are also examined by using statistical method, such as the density of states (DOS) per unit energy range as given by

$$D_n(\epsilon) = \frac{2}{8\pi^2} \int \delta(E_F - \epsilon_n(\mathbf{k})) d\epsilon \quad (3)$$

with the allowed wavevector in the n^{th} band energy range, $\varepsilon \leq \varepsilon_n(\mathbf{k}) \leq \varepsilon + d\varepsilon$ is just the volume of a \mathbf{k} -space primitive cell, divided by the volume per allowed wave vector,

$$\Delta k = 2\pi^3/V.$$

The transport coefficients of the TMOs are investigated for the optimized systems by using BoltzTraP code, a patching software of WIEN2k framework, which implements the linearized Boltzmann Transport Equation (BTE) [18] as given by,

$$\frac{\partial f_{\mu}(T, \mu)}{\partial t} = -v_{\alpha}(i, \mathbf{k}) \cdot \frac{\partial f_{\mu}(T, \mu)}{\partial \mathbf{r}} - \frac{e}{\hbar} \left(E - \frac{1}{c} v_{\alpha}(i, \mathbf{k}) \times H \right) \cdot \frac{\partial f_{\mu}(T, \mu)}{\partial k_{\alpha}} + \frac{\partial f_{\mu}(T, \mu)}{\partial t} \Big|_{\text{scattering}} \quad (4)$$

with $f_{\mu}(T, \mu) = \frac{1}{\exp[(\mu - E_F)/k_B T] + 1}$ is the Fermi-Dirac distribution for electron and

$v_{\alpha}(i, \mathbf{k}) = \frac{1}{\hbar} \frac{\partial \varepsilon_{i, \mathbf{k}}}{\partial k_{\alpha}}$ is the group velocity of the carriers.

From the first-principle, the Seebeck coefficient (S) and figure of merit (ZT) are calculated as,

$$ZT = \frac{\sigma_{\alpha\beta} S_{\alpha\beta}^2}{\kappa_{\alpha\beta}} T \quad (5)$$

Where ,

$$\sigma_{\alpha\beta}(T, \mu) = \frac{1}{\Omega} \int \bar{\sigma}_{\alpha\beta}(\varepsilon) \left[-\frac{\partial f_{\mu}(T, \mu)}{\partial \varepsilon} \right] d\varepsilon \quad (6)$$

is the electrical conductivity tensor,

$$\kappa_{\alpha\beta}(T, \mu) = \frac{1}{\Omega e^2 T} \int \bar{\sigma}_{\alpha\beta}(\varepsilon) (\varepsilon - \mu)^2 \left[-\frac{\partial f_{\mu}(T, \mu)}{\partial \varepsilon} \right] d\varepsilon \quad (7)$$

is the thermal conductivity tensor,

$$S_{\alpha\beta}(T, \mu) = \frac{1}{\Omega e T \sigma_{\gamma\alpha}(T, \mu)} \int \bar{\sigma}_{\gamma\beta}(\varepsilon) (\varepsilon - \mu) \left[-\frac{\partial f_{\mu}(T, \mu)}{\partial \varepsilon} \right] d\varepsilon \quad (8)$$

is the thermoelectric Seebeck coefficients,

And,

$$\bar{\sigma}_{\alpha\beta}(\varepsilon) = \frac{e^2}{N} \sum_{i, \mathbf{k}} \tau_{i, \mathbf{k}} v_{\alpha}(i, \mathbf{k}) v_{\beta}(i, \mathbf{k}) \delta(\varepsilon - \varepsilon_{i, \mathbf{k}}) \quad (9)$$

is the kernel of all transport coefficients, that is necessary for calculating the Figure of merit.

Where α and β are tensor indices, Ω , μ and N are the volume of the unit cell, chemical potential and number of \mathbf{K} -points implemented respectively.

Furthermore, the dynamical mean field theory (DMFT) can be applied for realistic picture of electronic system by using the Hubbard Hamiltonian for strongly correlated system as,

$$\hat{H} = \sum_{ijlm\sigma} t_{ijlm} \hat{c}_{il}^{\sigma\dagger} \hat{c}_{jm}^{\sigma} + \sum_{ilmno\sigma\sigma'} U_{ilmno} \hat{c}_{il}^{\sigma\dagger} \hat{c}_{im}^{\sigma\dagger} \hat{c}_{in}^{\sigma'} \hat{c}_{io}^{\sigma} \quad (10)$$

Where, $\hat{c}_{il}^{\sigma\dagger}$ (\hat{c}_{il}^{σ}) creates (annihilates) an electron with spin σ and orbital index l at lattice site i .

t_{ijlm} is the hopping amplitude between lattice sites i and j and orbitals l and m .

U_{ilmno} denotes a general local Coulomb interaction [19-21].

Mapping onto the Anderson impurity model Hamiltonian for DMFT calculation as

$$\hat{H}_{AIM} = \sum_{kl\sigma} \varepsilon_l(k) \hat{a}_{kl}^{\sigma\dagger} \hat{a}_{kl}^{\sigma} + \sum_{kl\sigma} [V_{lm}(k) \hat{a}_{kl}^{\sigma\dagger} \hat{c}_m^{\sigma} + h. c.] + \sum_{ilmno\sigma\sigma'} U_{ilmno} \hat{c}_{il}^{\sigma\dagger} \hat{c}_{im}^{\sigma\dagger} \hat{c}_{in}^{\sigma'} \hat{c}_{io}^{\sigma} \quad (11)$$

Where $\hat{a}_{kl}^{\sigma\dagger}$ (\hat{a}_{kl}^{σ}) are creation and annihilation operators for non-interacting conduction electrons at wave vector \mathbf{k} , which have a dispersion $\varepsilon_l(\mathbf{k})$ and hybridize with the localized interacting electrons $\hat{c}_m^{\sigma\dagger}$ via $V_{lm}(k)$.

The equation with the modeled Hamiltonian (11) can be solved by various kinds of impurity solvers, such as CT-QMC, DMRG, NCA, IPT etc.

The interacting Green function and hence the self energy, $\Sigma(\omega)$ can be calculated by using the Dyson equation as,

$$[G^0(\omega)]^{-1} = [G(\omega)]^{-1} + \Sigma(\omega) \quad (12)$$

The spectral function, which is associated with the imaginary part of Green function at a given momentum is a Dirac δ -function [22-25] as,

$$A(\mathbf{k}, \omega) = -\frac{1}{\pi} \text{Im}[G(\mathbf{k}, \omega)] = \delta(\omega - \varepsilon_{\mathbf{k}}) \quad (13)$$

And, the total local spectral function coincides with the Bethe density of states (DOS).

Turning on correlations, the spectral function has a Lorentzian profile as,

$$A(\mathbf{k}, \omega) = -\frac{1}{\pi} \left[\frac{\text{Im} \Sigma(\omega)}{(\omega + \mu - H_0(\mathbf{k}) - \text{Re}[\Sigma(\omega)])^2 + \text{Im}[\Sigma(\omega)]^2} \right] \quad (14)$$

The real part of the self-energy shows a shift of the non-interacting excitations, whereas the imaginary part of self-energy indicates the broadening of the quasiparticles excitations. Since, the self-energy strongly depends on the frequency and in the case of the Mott insulator, it will lead to a notable transfer of spectral weights.

The maximum likelihood of spectral function, $A(\omega)$, is obtained by maximizing the probability using Bayesian theorem[26] as,

$$P[A(\omega)|G(\omega)] = \frac{P[G(\omega)|A(\omega)]}{P[G(\omega)]} P[G(\omega)] \sim e^{\alpha S - \frac{1}{2} \chi^2} \quad (15)$$

The Green function, $G(\omega)$ is data obtained from the DMFT calculation using CT-QMC-hybridization technique as the impurity solver. The reliable features of the spectral function, such as height and width of the central peak, and the overall weight and position of the Hubbard bands are obtained by using the maximum entropy method with the optimized value of adjustable parameter, α that will have the required information of the system concerned. The algorithm first computes the solution to $\min(\chi^2 - \alpha S)$ for a large range of α . The location of the optimal value of α can be found by plotting a graph between $\log_{10}(\chi^2)$ as a function of $\log_{10}(\alpha)$, which gives the maximum likelihood of the required information lies somewhere in the portion of information fitting region of the logistic regression curve (sigmoid curve).

2.2 Computational Details and Experimental Information

The electronic structure, density of states (DOS), electronic charge density distribution and transport behaviours the cubical TMO systems are studied using the full potential-linearized augmented plane wave (FP-LAPW) with local orbitals (lo) based on DFT frameworks. The Kohn-Sham equations have been solved by the method of self-consistent total energy calculations within the generalized gradient approximation (GGA) developed by three scientists Perdew, Burke and Ernzerhof [26, 27] for

approximating the electronic exchange and correlation effects.

We have employed the various schemes, such as GGA+U, GGA+U+J, GGA+SOC, GGA+mBJ etc. for improving the underestimated electronic structure based on the conventional density functional theory [28,29].

Despite the whole story of DFT calculation, we have employed the dynamical mean field theory (DMFT) with the continuous time quantum Monte Carlo (CT-QMC) -hybridization technique as the impurity solver for computing the realistic picture of electronic structure of TMOs, so as to explore the Mott-Hubbard metal-insulator transition [30,31]. The statistical inferences are implemented by applying Maximum Entropy Model for obtaining the spectral density distribution from DMFT data [32, 33].

The Mott-Hubbard band splitting of strongly correlated system have been investigated by using dynamical mean field theory (DMFT)

The theoretical study of MIT is done using the density functional theory (DFT) and the dynamical mean field theory (DMFT) [34, 35]. A band controlled transition metal oxide system, $\text{La}_{(1-x)}\text{Sr}_x\text{TiO}_3$, which are reconstructed by site substitution of extended pristine superlattice of cubic perovskite, SrTiO_3 . The MIT phase transition are investigated for the strongly correlated parameter, U and the thermodynamic parameter, β through DFT + DMFT [36, 37].

In the present study, we have used Monk-horst pack of $7 \times 7 \times 7$ k-mesh grid for the pristine TMOs unit cell. The k-mesh grid of $13 \times 13 \times 2$ for both of the superstructures is used for DFT calculation with the energy and charge convergence criteria for the entire systems are 10^{-5} eV and 10^{-3} e respectively. And the force convergence criterion is 0.05 eV/Å used for the entire calculation.

Furthermore, the BoltzTraP codes are used for computing the thermal conductivity, electrical conductivity, Seebeck coefficients and figure of merit (ZT) etc. of the $\text{La}_{1-x}\text{Sr}_x\text{TiO}_3$ superlattices.

The transport properties of interfaces of LaTiO_3 and SrTiO_3 i.e. Mott and band insulators have shown high mobility of electron gas due to charge redistribution of substitutional dopant such as La or Sr, by charge transfer, crystal polarity etc. [38]. All the heterostructures are grown on SrTiO_3 (100) substrates preannealed at 900°C and LaTiO_3 films were grown using pulsed laser deposition at a substrate temperature of 500°C and an oxygen

background pressure of 10^{-6} Torr. using polycrystalline $\text{La}_2\text{Ti}_2\text{O}_7$ target. All of the heterostructures grown found to be metallic on measuring the transport and Hall measurement of the system upto 5 T of magnetic field [39].

3. RESULTS AND DISCUSSION

3.1 Structural Stability and Optimization

The optimized parameters for the given TMOs (systems) are obtained through energy minimization technique using first-principle method.

The cubic phase of SrTiO_3 , which belongs to the space group pm-3m is known to be a band insulating material. The cubic unit cell contains one molecule with the Sr-atom sitting at the origin (0.0, 0.0, 0.0)a, the Ti-atom at the body center (0.5, 0.5, 0.5)a and the three O-atoms at the three face centers (0.5, 0.5, 0.0)a, (0.0, 0.5, 0.5)a, and (0.5, 0.0, 0.5)a; the lattice constant is $a = 7.297$ bohr. Similarly, the cubic phase unit cell of LaTiO_3 contains one molecule with the La-atom sitting at the origin (0.0, 0.0, 0.0)a, the Ti-atom at the body center (0.5, 0.5, 0.5)a and the three O-atoms at the three face centers (0.5, 0.5, 0.0)a, (0.0, 0.5, 0.5)a, and (0.5, 0.0, 0.5)a; the lattice constant is $a = 7.100$ bohr (1 bohr = 0.529 Å) [40,41].

In this study the convergence parameters, such as K-points, rKmax and Gmax values for SrTiO_3 are obtained as 500, 7.0 and 17.0 respectively along with RMT-values 2.50 for Sr-atom, 1.87 for Ti-atom and 1.69 for O-atoms respectively. Similarly, the convergence parameters, such as K-points, rKmax and Gmax values for LaTiO_3 are obtained as 500, 7.5 and 18.0 respectively along with RMT-values 2.50 for Sr-atom, 1.82 for Ti-atom and 1.65 for O-atoms respectively.

The crystal structure of SrTiO_3 and LaTiO_3 (inset) with their lattice parameters optimization curves is shown in Fig. 2.

The optimized unitcell of LaTiO_3 is promoted to $1 \times 1 \times 5$ supercell, so as to study the effect of the site substitution of Sr-atom on LaTiO_3 supercell on the electronic structure and transport properties of $\text{La}_{(1-x)}\text{Sr}_x\text{TiO}_3$ superlattice system[42-44]. The superlattice, $\text{La}_{0.80}\text{Sr}_{0.20}\text{TiO}_3$ system of space group p4/mm with lattice parameters, $a = b = 3.592$ Å and $c = 18.126$ Å with RMT values for La-, Sr-, Ti-, O- are found to be 2.50, 2.36, 1.65 and 1.49 respectively. For superlattice, $\text{La}_{0.20}\text{Sr}_{0.80}\text{TiO}_3$ system of space group p4/mm with lattice parameters, $a = b = 3.853$ Å and $c = 19.445$ Å with RMT values for La-, Sr-, Ti-, O- are found to be 2.50, 2.50, 1.77 and 1.60 respectively.

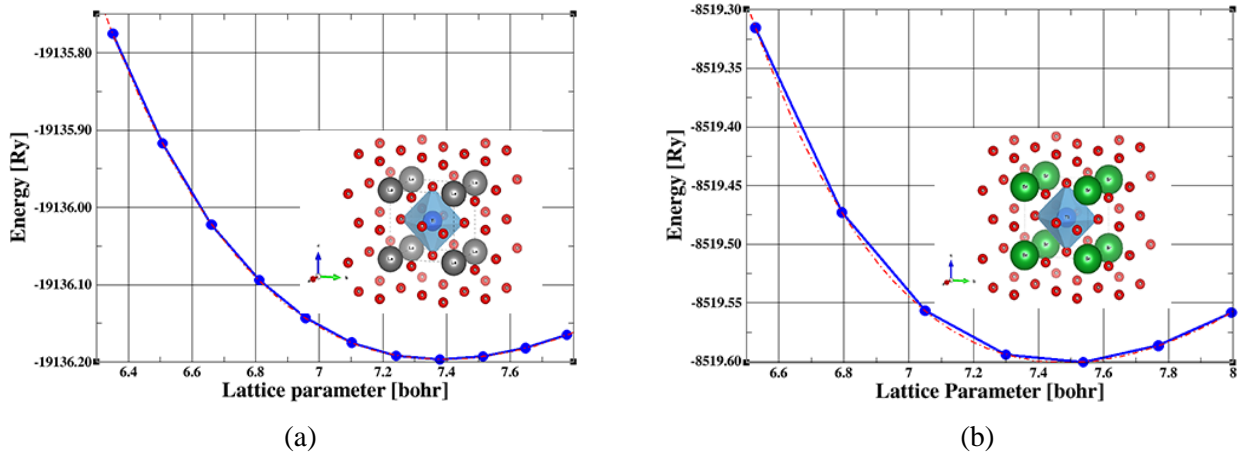


Fig. 2: (color online) The lattice parameter optimization curves of the cubic phases of (a) LaTiO_3 and (b) SrTiO_3 systems (crystal structures in inset).

3.2 Electronic band structure and Density of States (DOS)

The optimized pristine SrTiO_3 and LaTiO_3 systems have been taken through self-consistent calculation for investigating their electronic structure and transport properties [45-47]. The ground state

calculation was performed through the energy minimization technique for the given system. The calculated energy band structure for cubic phases SrTiO_3 is shown in Fig. 3(a).

In the case of LaTiO_3 system Fig. 3(b), it is observed that the band at around the Fermi-level is

mostly contributed by e_g and t_{2g} orbitals of transition metals (Ti). The crystal field and the electrostatic interaction between the V-cation and

the non-bonding O-2p electrons that produces the splitting of d-orbitals [48].

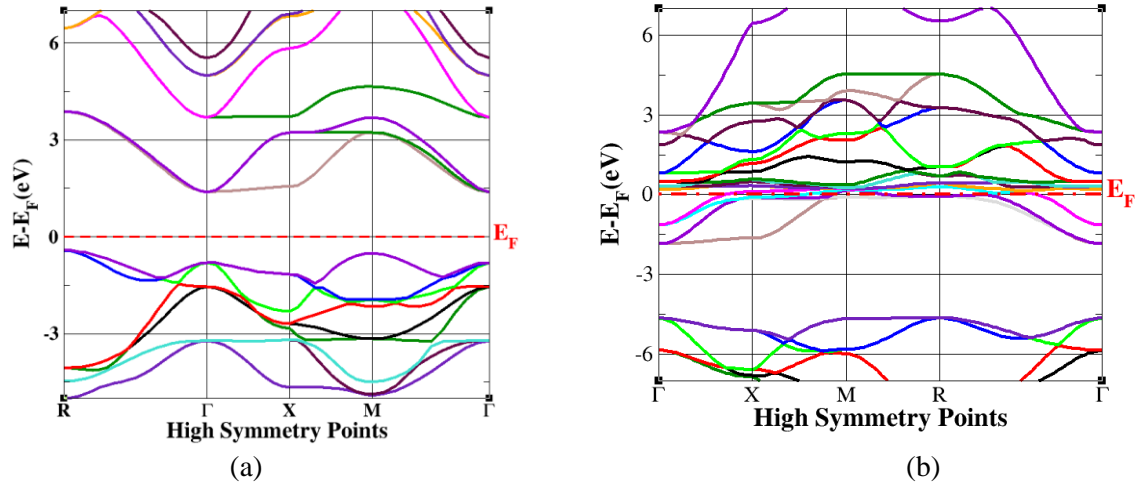


Fig. 3: (color online) The band structure plotted between the total energy versus the various symmetry points for SrTiO_3 (left) and LaTiO_3 (right) unit cell.

There are three doubly degenerate valence bands are derived mainly from the oxygen 2p orbital which are separated by a direct gap of 2.20 eV (at the Γ point) from the transition-metal d-derived (Ti) conduction band. This band gap is corrected to 3.423 eV by applying the modified Beck-Johnson interaction potential. It is somewhat lower than the experimental band gap of 3.75 eV for SrTiO_3 [49, 50].

The fatbandstructures of the Ti-atom of LaTiO_3 system is shown in Fig. 4.

The bandstructure of LaTiO_3 is shifted by introducing the Coulomb interaction U and it is shifted further with higher value of U and Hund's exchange interactions, J and along with spin-orbit coupling, (SOC) as in Fig. 5 (a),(b).

It has been revealed that the introduction of modified Beck-Johnson interaction potential with GGA calculation for the strongly correlated system, SrTiO_3 increases the band gap [49- 51].

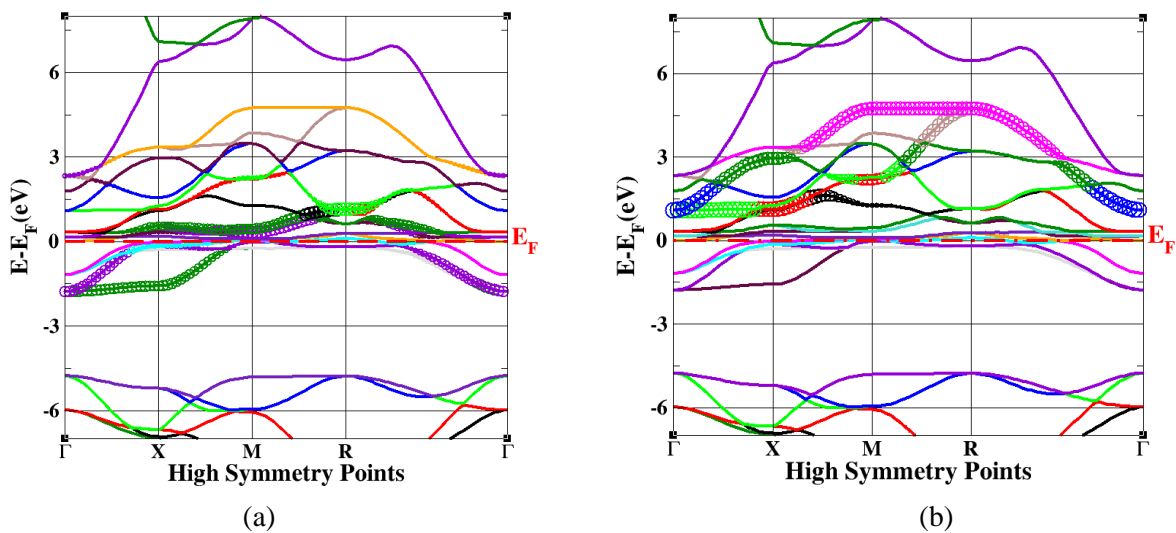


Fig. 4: (color online) Fatbandstructures of (a) Ti- t_{2g} -orbitals on (left) and (b) Ti- e_g -orbitals on (right) of LaTiO_3

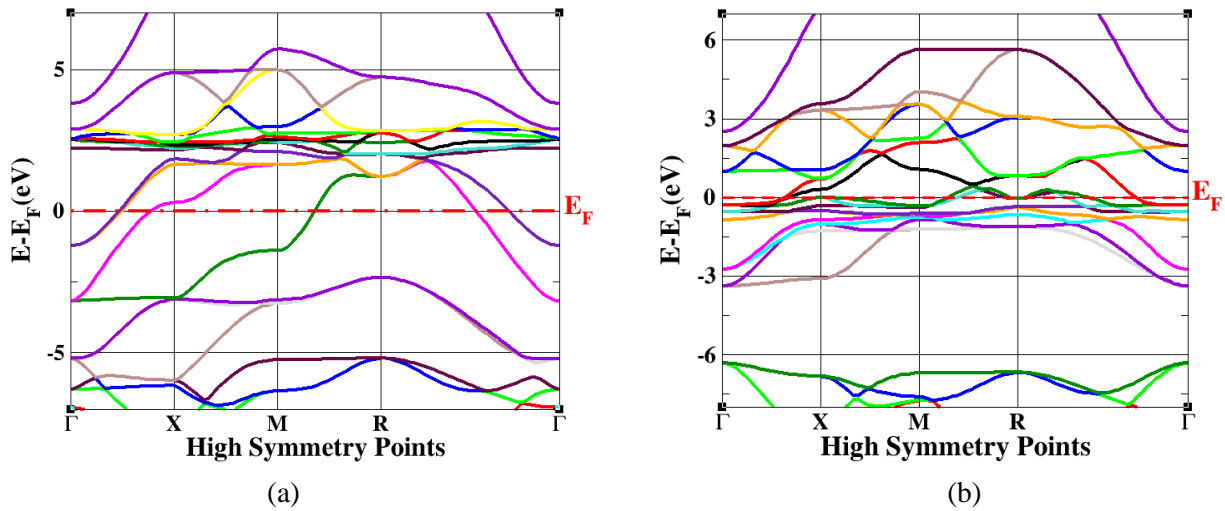


Fig. 5: (a) (color online) The shifting of band of $LaTiO_3$ with, $U=2.11\text{eV}$ and $J=0.20\text{eV}$ (b) The effect of spin-orbit coupling (SOC) in $LaTiO_3$ system.

The electronic bandstructure of superlattice, $La_{0.80}Sr_{0.20}TiO_3$ reveals that the system is metallic and the introduction of Coulombian interaction, U and exchange interaction, J along with spin-orbit

coupling (SOC) seems to be the important parameters for determining the electronic structures of the materials as shown in Fig. 6.

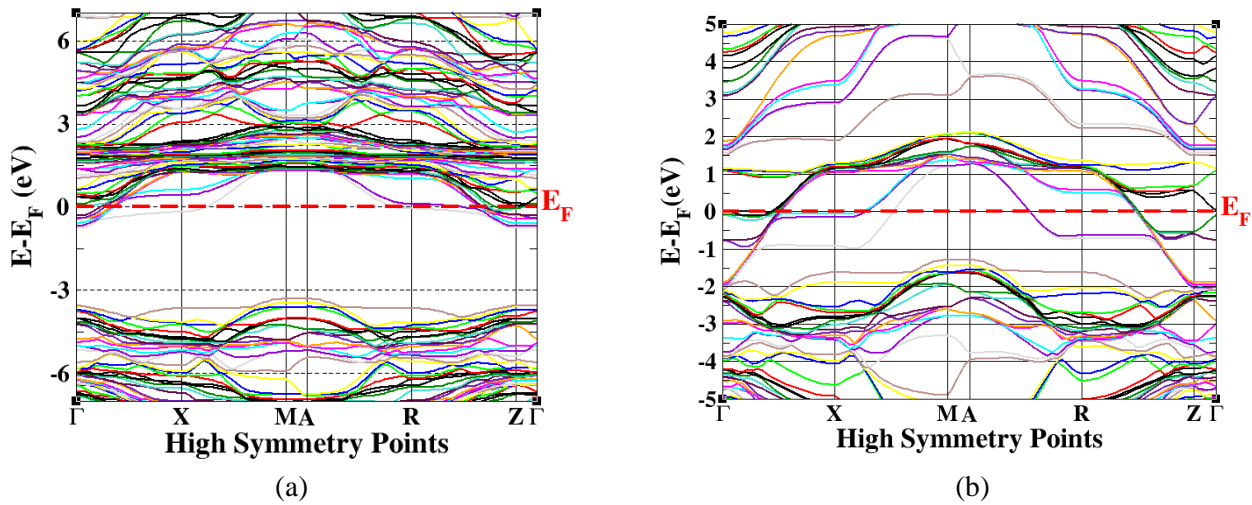


Fig. 6: (a) (color online) Bandstructure of the $La_{0.80}Sr_{0.20}TiO_3$ system without U and J (b) Bandstructure of same system with $U=2.11\text{eV}$, $J=0.25\text{eV}$ and SOC.

The density of states (DOS) is essentially the number of different states at a particular energy level that electrons are allowed to occupy i.e the number of electronic states per unit volume per unit energy is a useful computational tools to find the electronic structures of materials in the ground states [14,15]. In order to find the constituent atomic contribution in the electronic structure and magnetic behaviors of the system, the partial

density of states (PDOS) have been employed with consideration of the spin polarization, so as to calculate the contribution on electronic structure of individual atom. The DOS in the vicinity of the Fermi level within the band structure of $LaTiO_3$ were attributed mostly to these octahedral hybrid orbitals. In Fig. 7 (a) The DOS of $SrTiO_3$ with mBJ interaction is consistent with the experimental result [49-51].

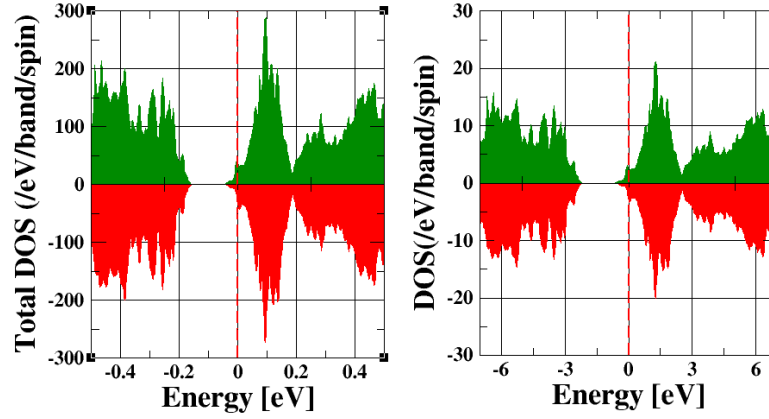


Fig. 7: (color online) The DOS of $\text{La}_{0.20}\text{Sr}_{0.80}\text{TiO}_3$ system for both up and down spin channels.

The symmetrical distribution of DOS for both channels of the superstructures indicate that these systems are non-magnetic or paramagnetic in behaviour.

3.3 Charge Density Distribution and Fermi Surface of the system

The charge density 3D plot with 2D contour plot (in inset) of LaTiO_3 are illustrated Fig. 8(a), and 8(b) respectively.

The strong covalent bondings between Ti- and O-atoms have been observed due to the overlap (hybridization) of O-2p and Ti-3d orbitals, which is in good agreement with the previously published papers of perovskites compounds [52,53]. The 2D-contour plot shows that the chemical bonding is mainly takes place nearest neighboring atoms.

The 3D-electron density distribution map for LaTiO_3 as shown in Fig. 8(a), with the planes (011)

confirms that the electron density distribution is mainly localized near the ionic cores as expected, the high peaks of 3D plots shows the contribution of Ti-atoms, which is symmetric about the core of the atoms.

The study of Fermi surface of the system also supports the results obtained through band structure and DOS structure of the system. The Fermi surfaces around the various atomic lattice sites, constituted by several electron and hole orbits are demonstrated for the LaTiO_3 systems as shown in Fig. 8(b). The Fermi surfaces constituted by 20-40 band levels are shown (inset-1) and the actual Fermi surfaces of 30-51 band levels with the tentacles, called monster is shown (inset-2). Furthermore, the Fermi level, E_f crossing through the energy bands of 30-40 band levels of the system is demonstrated in Fig. 8(b) [54, 55].

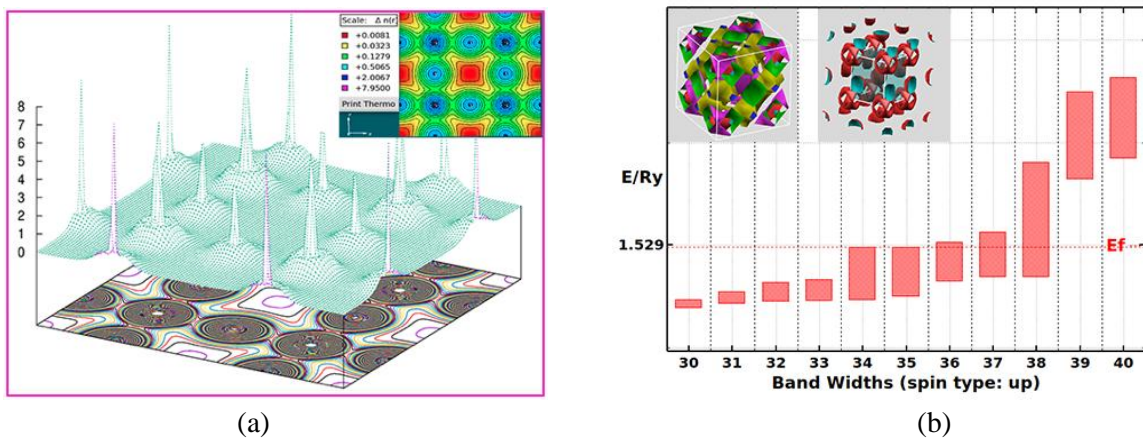


Fig. 8: (color online) (a) The 3D charge density plot along with the 2D contour plot (inset) of LaTiO_3 in (011) plane (b) The Fermi level crossing through energy bands of 30-40 band levels of the LaTiO_3 system with its Fermi surface and the actual Fermi surfaces of 30-51 band levels with the tentacles (inset).

3.4 Electronic Structure by DMFT

The conventional DFT calculation is not able to predict the realistic picture of electronic structure for strongly correlated materials, so we have employed the dynamical mean field theory (DMFT) with continuous time quantum Monte Carlo (CT-QMC) hybridization technique as the impurity solver for finding the electronic structure of the

transition metal oxides [56-59].

The characteristic variation of Green function of imaginary time, ($\tau = it$) with the variation of Coulombian interaction (U) for the thermodynamic parameter, $\beta=6(\text{eV})^{-1}$ is shown in Fig. 9(a) and the corresponding Fourier transform of $G(\omega)$ for the DMFT data showing the MIT with kinks at near minimum frequency as shown in Fig.9(b).

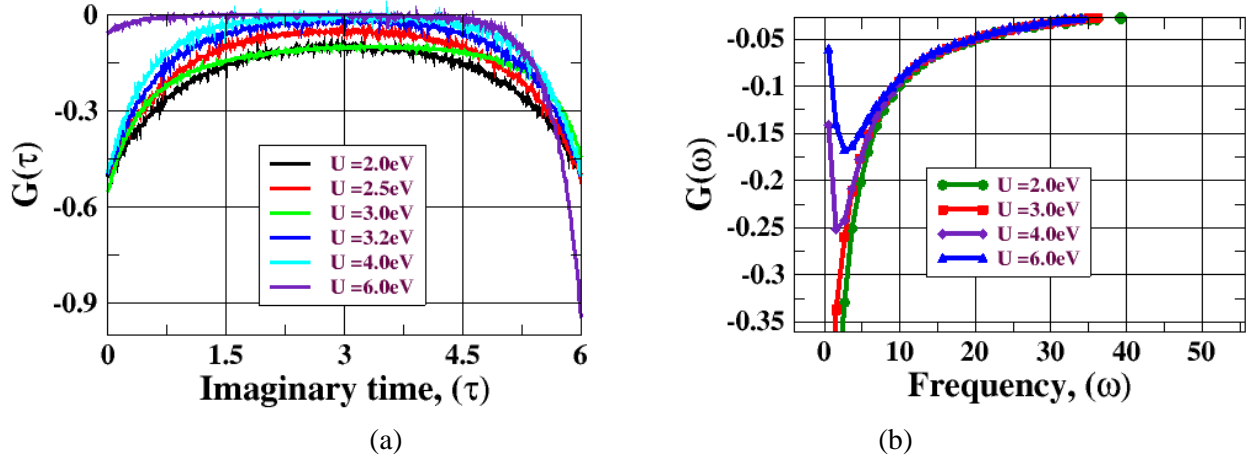


Fig. 9: (color online) (a) The variation of Green function vs. imaginary time with various values of U (b) the corresponding spectral density vs. frequency showing the Mott-Hubbard splitting with $U = 4.0$ eV.

The complete metal-insulating phase transition is observed for $U = 2.5$ eV and $\beta = 6(\text{eV})^{-1}$ for $LaTiO_3$ as shown in Fig. 10(a).

Similarly, the characteristic variation of the Green function of frequency, clearly supports the metallic and insulating phases of the materials as shown in

Fig. 10(a). The oscillation of self energy, $\Sigma(\omega)$ oscillation with frequency is shown in Fig. 10(b) showing that there is no change in self energy, $\Sigma(\omega)$ with the variation of the Coulombian parameter, U .

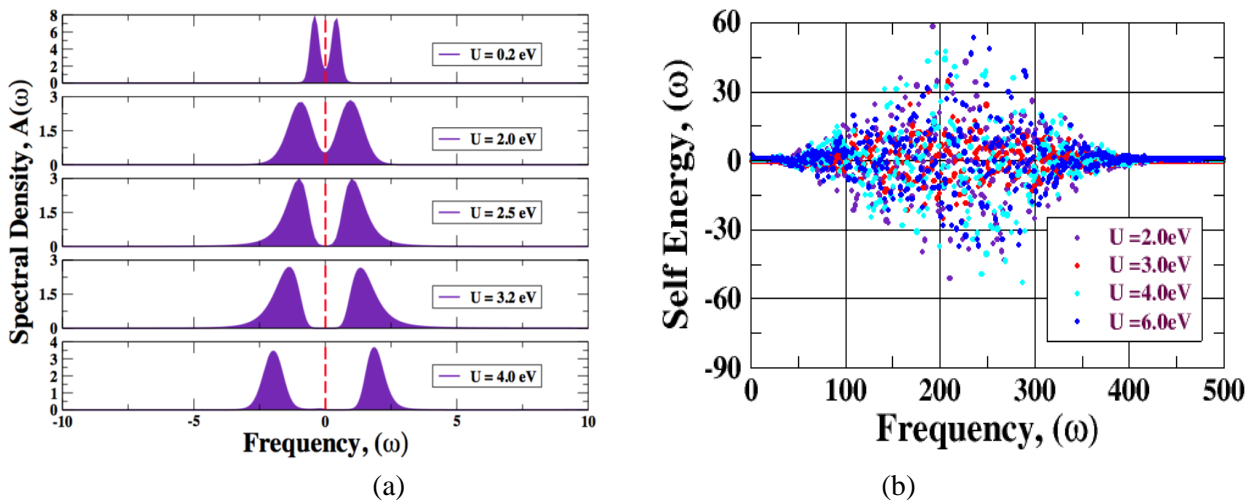


Fig. 10: (color online) (a) The variation of spectral density, $A(\omega)$ vs. frequency for various U values (b) The self-energy vs. frequency.

Furthermore, the spectral density, $A(\omega)$, which is obtained from the Green function, $G(\tau)$ of superlattice, $\text{La}_{0.80}\text{Sr}_{0.20}\text{TiO}_3$ system using the Maximum Entropy model of data analysis algorithm. The metallic phase with quasi-particle peak for the superlattice, $\text{La}_{0.80}\text{Sr}_{0.20}\text{TiO}_3$ is obtained for $U = 3.0\text{eV}$ and $\beta = 6(\text{eV})^{-1}$ as shown in Fig.11(a). Furthermore, on increasing the Coulombian parameter, U for a constant $\beta = 10 (\text{eV})^{-1}$, the system undergoes metal-insulator transition as shown in Fig. 11(b).

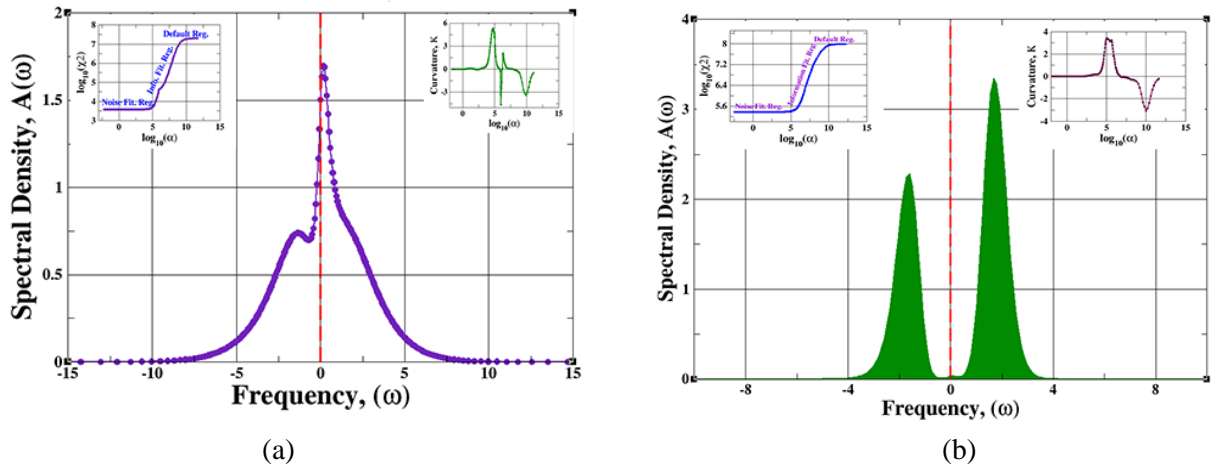


Fig. 11: (color online) (a) Green function of frequency vs. frequency showing the quasi-particle peak for $\text{La}_{0.80}\text{Sr}_{0.20}\text{TiO}_3$. The logistic regression curve or sigmoid curve (inset), which is the cross validation error analysis of calculation. (b) The metal insulator phase transition for $U = 3.5 \text{ eV}$ and $\beta = 10 \text{ eV}^{-1}$ for superlattice, $\text{La}_{0.20}\text{Sr}_{0.80}\text{TiO}_3$ and the logistic regression curve along with the curvature of it (inset).

3.5 Transport properties of SrTiO_3 and LaTiO_3

The various properties of materials, such as the transport properties are also associated with the electrons and lattice interactions. Here, the density functional theory (DFT) have employed for investigating electrical, thermal, and thermoelectric behaviours of TMOs based on the BoltzTrap module [11,61]. The ever-increasing computing power has made the first principles calculation more and more accurate and straightforward. As the transport properties of the materials are electronic bandstructure dependent quantities, the BoltzTrap codes, which implements the linearized Boltzmann transport equation is applicable to compute various transport coefficients including intermetallic compounds, high T_C superconductor and thermoelectric materials etc.

The study of transport properties are highly useful to predict and design a new materials for diverse fields, such as the superconductors, transparent

conductors, transparent insulators, inter-metallic phases as well as the efficient thermometric materials [18, 61].

The maximum likelihood of the spectral function $A(\omega)$, having a realistic features of central peak, height, width and the overall weight, is obtained by using the optimal value of the adjustable parameter, α [60].

The cross validation error is done for obtaining a good and reliable spectral function with the maximum entropy method. The location of the optimal α can be found by choosing its value from the information fitting region of the logistic regression (sigmoid) curve as shown (inset) Fig.11 (b).

The significant variation of electrical conductivity, (σ/τ) and thermal conductivity, (κ) with temperature are observed for the different proportion of Sr-atom in the supercells for a constant chemical potential, $\mu = 0.821 \text{ eV}$. But, the change of electrical conductivity varies slowly (not significantly) with temperature whereas the thermal conductivity varies significantly with temperature along with the various proportions of Sr-atoms on the supercells.

The comparison of Figure of merit (ZT) vs. chemical potential (μ) at room temperature shows that the $ZT \sim 1.78$ for a system with 40% of Sr-ions at around $\mu = -0.7 \text{ eV}$. A remarkable thermoelectric phase transitions are observed for Seebeck Coefficient at temperature, 300 K for the systems with higher proportion of Sr-ions.

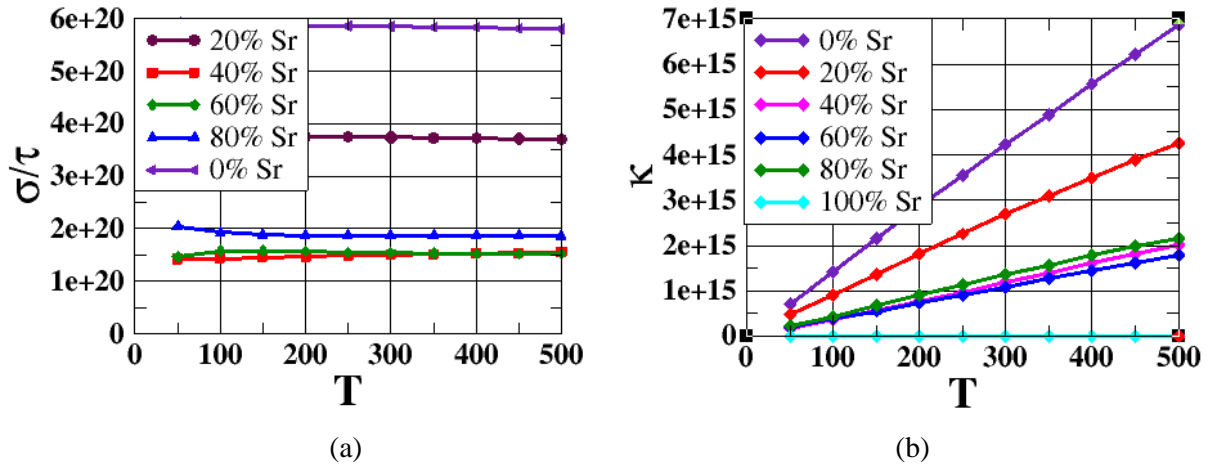


Fig. 12: (color online) (a) The variation of electrical conductivity with temperature (b) The variation thermal conductivity with temperature for different proportion of Sr-ions having the same chemical potential, $\mu = 0.821$ eV.

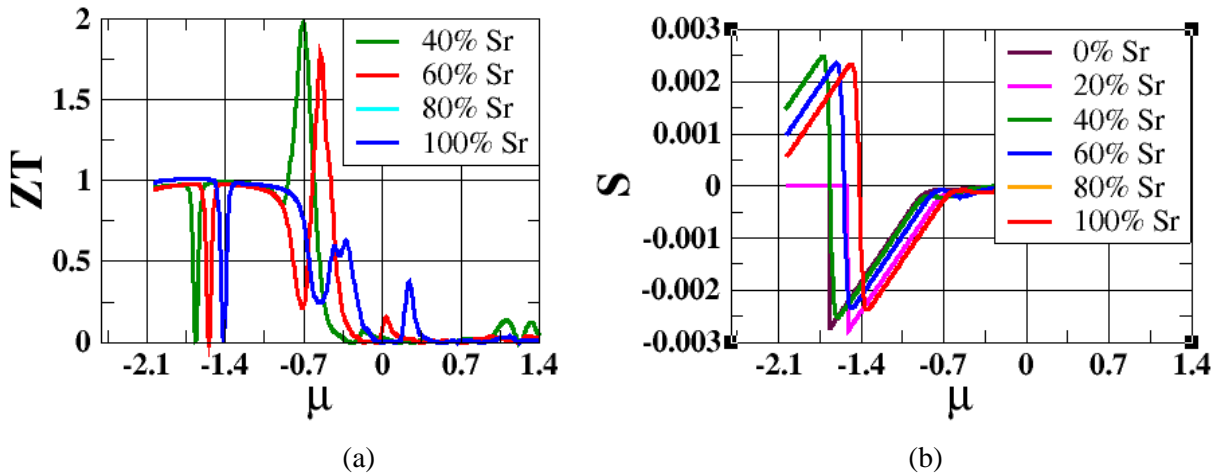


Fig. 13: (color online) (a) The comparison of Figure of merit (ZT) with chemical potential (μ) at room temperature for various proportion of Sr-ions (b) The thermoelectric phase transition are observed for Seebeck Coefficient vs. chemical potential (μ) at temperature, 300 K.

The ultimate study of finding these transport properties is to investigate the possibility of promising thermoelectric materials by knowing the Figure of merit (transport coefficient) as shown in Fig.13. The higher the value of ZT confirms that the better the potential materials for thermoelectric application for recycling the wastage of heat energy [62,63].

4. CONCLUSIONS

The electronic structure and transport properties of pristine $LaTiO_3$ and $SrTiO_3$ along with their superlattice system have been studied using conventional DFT and DMFT.

The shifts in the energy bands of TMOs are clearly observed by introducing the Coulombian interaction (U), Hund's exchange (J) and spin-orbit couplings (SOC). The calculated band gap for $SrTiO_3$ is found to be 3.423 eV with mBJ interaction potential, which is close enough to the experimental information.

The dynamical mean field theory (DMFT) with CT-QMC-hybridization as impurity solver have employed to investigate metal-insulator (MIT) phase transition of pristine $LaTiO_3$ and the superlattice of $La_{(1-x)}Sr_xTiO_3$ system. The correlation parameters for the pristine $LaTiO_3$ for a distinct metal-insulator transition (MIT) are

obtained for $U = 2.5$ eV, $\beta = 6(\text{eV})^{-1}$ and $J = 0.60$ eV. Whereas these parameters are found to be $U = 3.2$ eV, $\beta = 10 (\text{eV})^{-1}$ and $J = 0.60$ eV for the $\text{La}_{0.80}\text{Sr}_{0.20}\text{TiO}_3$ system and $U = 3.5$ eV, $\beta = 10 (\text{eV})^{-1}$ and $J = 0.60$ eV for the $\text{La}_{0.20}\text{Sr}_{0.80}\text{TiO}_3$ system respectively. The spike of the quasiparticles at around the Fermi level of $\text{La}_{0.80}\text{Sr}_{0.20}\text{TiO}_3$ system is observed for $U = 3.0$ eV, $\beta = 6(\text{eV})^{-1}$, $J = 0.60$ eV.

The thermal conductivity varies significantly with the temperature but the electrical conductivity is observed to be remains same with temperature for a system. The higher value of Figure of merit, $ZT \sim 1.75$ and 1.99 are calculated for the systems with 40% and 60% of the Sr-ions. The thermoelectric phase transition with chemical potential, μ are observed at around $\mu \sim -1.4$ eV for system with higher proportion of Sr-ions. Thus, the $\text{La}_{(1-x)}\text{Sr}_x\text{TiO}_3$ systems are the potential candidates for the thermoelectric application at higher temperature.

5. ACKNOWLEDGEMENT

The authors gratefully acknowledged UGC and NAST for their financial supports. We acknowledged the supercomputer center of KU for supporting in parts through the computational facility. The authors gratefully acknowledged the ABINIT and ALPS codes library in parts for DMFT calculations.

REFERENCES

- [1] Imada, M.; Fujimori, A.; & Tokura, Y. Metal-insulator transitions. *Reviews of modern physics*, **70**(4): 1039 (1998).
- [2] Bell, C.; Harashima, S.; Kozuka, Y., *et al.* Dominant mobility modulation by the electric field effect at the $\text{LaAlO}_3/\text{SrTiO}_3$ interface. *Phys. Rev. Lett.*, **103**: 226802 (2009).
- [3] Larson, P.; Popović, Z. S.; & Satpathy, S. Lattice relaxation effects on the interface electron states in the perovskite oxide superlattices: LaTiO_3 monolayer embedded in SrTiO_3 . *Physical Review B*, **77**(24): 245122 (2008).
- [4] Edmondson, B. I. & Ekerdt, J. G. Effect of SrTiO_3 oxygen vacancies on the conductivity of $\text{LaTiO}_3/\text{SrTiO}_3$ superlattices. *Journal of Applied Physics*, **124**(18): 185303 (2018).
- [5] Scafetta, Mark Dominic. *Optical Properties and Electronic Structure of non- d^0 Perovskite Oxide Epitaxial Films and Superlattices*. Drexel University (2015).
- [6] Kaphle, G. C.; Adhikari, N. & Mookerjee, A. Study of Spin Glass Behavior in Disordered $\text{Pt}_x\text{Mn}_{1-x}$ Alloys: An Augmented Space

- Recursion Approach. *Advanced Science Letters*, **21**(9): 2681-2687 (2015).
- [7] Held, K., & Vollhardt, D. Realistic investigations of correlated electron systems with LDA+DMFT. *physica status solidi (b)*, **243**(11): 2599-2631(2006).
- [8] Nekrasov, I. A., & Vollhardt, D. Calculation of photoemission spectra of the doped Mott insulator using LDA+ DMFT (QMC). *The European Physical Journal B-Condensed Matter and Complex Systems*, **18**(1): 55-61 (2000).
- [9] Blümer, N. *Mott Hubbard Metal Insulator Transition and Optical Conductivity in High Dimensions*. Shaker (2003).
- [10] Ramakrishnan, T. V. Strongly correlated electrons in solids. *Current Science* (00113891), **95**(9): (2008).
- [11] Zhang, X., & Zhao, L. D. Thermoelectric materials: Energy conversion between heat and electricity. *Journal of Materiomics*, **1**(2): 92-105(2015).
- [12] Saeed, Y. *Tuning the Transport Properties of Layered Materials for Thermoelectric Applications using First-Principles Calculations* (Doctoral dissertation) (2014).
- [13] Takagi, H., & Hwang, H. Y. An emergent change of phase for electronics. *Science*, **327**(5973): 1601-1602 (2010).
- [14] Scheiderer, P. & Claessen, R. *et al.* Tailoring materials for mottronics: excess oxygen doping of a prototypical mott insulator. *Advanced Materials*, **30**(25): 1706708(2018).
- [15] Kohn, W., & Sham, L. J. Self-consistent equations including exchange and correlation effects. *Physical Review*, **140**(4A): A1133 (1965).
- [16] Blaha, P.; Schwarz, K.; Madsen, G. K.; Kvasnicka, D. & Luitz, J. wien2k. An augmented plane wave+ local orbitals program for calculating crystal properties (2001).
- [17] Datta, S.; Kaphle, G. C.; Baral, S. & Mookerjee, A. Study of morphology effects on magnetic interactions and band gap variations for 3 d late transition metal bi-doped ZnO nanostructures by hybrid DFT calculations. *The Journal of chemical physics*, **143**(8): 084309 (2015).
- [18] Shi, X.; Yang, J.; *et al.* Multiple-filled skutterudites: high thermoelectric figure of merit through separately optimizing electrical and thermal transports. *Journal of the American Chemical Society*, **133**(20): 7837 (2011).
- [19] Mott, N. F. *Proc. Phys. Soc. A*, **62**: 416 (1949).
- [20] Mahmood, A., & Khan, S. U. D. First-principles study of electronic, optical and thermoelectric properties in cubic perovskite materials AgMO_3 ($M = \text{V}, \text{Nb}, \text{Ta}$). *Modern Physics Letters B*, **28**(10): 1450077 (2014).

- [21] Hubbard, J.; Electron Correlations in Narrow Energy Bands, Proc. Roy. Soc. A **276**: 238 (1963).
- [22] Held, K. Electronic structure calculations using dynamical mean field theory. Advances in physics, **56**(6): 829-926 (2007).
- [23] Gull, E. Continuous-time quantum Monte Carlo algorithms for fermions (Doctoral dissertation, ETH Zurich) (2008).
- [24] Paul, A., & Birol, T. Applications of dft+ dmft in materials science. Annual Review of Materials Research, **49**: 31-52 (2019).
- [25] Nekrasov, I. A., Anisimov, V. I. *et.al.* Comparative study of correlation effects in CaVO_3 and SrVO_3 . Physical Review B, **72**(15): 155106 (2005).
- [26] Bergeron, D. and Tremblay, A.-M. S. Phys. Rev. E **94**: 023303 (2016).
- [27] Perdew, J. P.; Burke, K., & Ernzerhof, M. Generalized gradient approximation made simple. Physical review letters, **77**(18): 3865 (1996).
- [28] Martin, R. M. Electronic structure: basic theory and practical methods. Cambridge university press (2004).
- [29] Mizutani, U. Introduction to the electron theory of metals. Cambridge University Press (2001).
- [30] Kaphle, G. C.; Ganguly, S., *et.al.* "A study of magnetism in disordered Pt-Mn, Pd-Mn and Ni-Mn alloys: an augmented space recursion approach. Journal of Physics Condensed Matter, **24**(29): 295501 (2012).
- [31] Georges, A.; Kotliar, G.; Krauth, W., & Rozenberg, M. J. Dynamical mean-field theory of strongly correlated fermion systems and the limit of infinite dimensions. Reviews of Modern Physics, **68**(1): 13 (1996).
- [32] Okamoto, S. & Millis, A. J. Theory of Mott insulator–band insulator superlattices. Physical Review B, **70**(7): 075101 (2004).
- [33] Fuchs, S. *Thermodynamic and spectral properties of quantum many-particle systems* (Doctoral dissertation, Niedersächsische Staats-und Universitätsbibliothek Göttingen) (2011).
- [33] Dymkowski, K. Strain-induced insulator-to-metal transition in d^1 perovskite systems within density functional theory plus dynamical mean field theory (Doctoral dissertation, ETH Zurich) (2015).
- [34] Backes, S. *Density Functional Theory and Dynamical Mean-field Theory: A Way to Model Strongly Correlated Systems* (Doctoral dissertation, Universitätsbibliothek Johann Christian Senckenberg) (2017).
- [35] Assaad, F. F. 7 Continuous-time QMC Solvers for Electronic Systems in Fermionic and Bosonic Baths. *DMFT at 25: Infinite Dimensions*, **51**: (2014).
- [36] Hirayama, S.; Imada, M. *et.al.* "Ab initio Low-energy model of transition-metal-oxide superlattice $\text{LaAlO}_3/\text{SrTiO}_3$." Journal of the Physical Society of Japan **81**.8: 084708 (2012).
- [37] Hosoda, M., ...& Hwang, H. Y. Compositional and gate tuning of the interfacial conductivity in $\text{LaAlO}_3/\text{LaTiO}_3/\text{SrTiO}_3$ superlattices. Applied Physics Letters, **102**(9): 091601 (2013).
- [38] Ohtsuka, R.; Matvejeff, M.; Nishio, K.; Takahashi, R., & Lippmaa, M. Transport properties of $\text{LaTiO}_3/\text{SrTiO}_3$ heterostructures. *Applied Physics Letters*, **96**(19): 192111 (2010).
- [39] Nishio, K.; Matvejeff, M.; Takahashi, R.; Lippmaa, M.; Sumiya, M.; Yoshikawa, H. & Yamashita, Y. Delta-doped epitaxial La: SrTiO_3 field-effect transistor. *Applied Physics Letters*, **98**(24): 242113(2011).
- [40] Piskunov, S.; Heifets, E.; Eglitis, R. I., & Borstel, G. Bulk properties and electronic structure of SrTiO_3 , BaTiO_3 , PbTiO_3 perovskites: an ab initio HF/DFTstudy. *Computational Materials Science*, **29**(2): 165-178 (2004).
- [41] Sclauzero, G.; Dymkowski, K., & Ederer, C. Tuning the metal-insulator transition in d^1 and d^2 perovskites by epitaxial strain: A first-principles-based study. *Physical Review B*, **94**(24): 245109 (2016).
- [42] Biscaras, J.; & Lesueur, J. Two-dimensional superconducting phase in $\text{LaTiO}_3/\text{SrTiO}_3$ superlattices induced by high-mobility carrier doping. Physical review letters, **108** (24): 247004 (2012).
- [43] Yoshida, C.; & Yokoyama, N. Electric field effect in $\text{LaTiO}_3/\text{SrTiO}_3$ superlattice. Japanese journal of applied physics, **35**(11R): 5691(1996).
- [44] Christen, H. M.; Kim, D. H., & Rouleau, C. M. Interfaces in perovskite superlattices. Applied Physics A, **93**(3): 807-811 (2008).
- [45] Ohtomo, A., & Hwang, H. Y. A high-mobility electron gas at the $\text{LaAlO}_3/\text{SrTiO}_3$ heterointerface. Nature, **427**(6973): 423(2004).
- [46] Ohtsuka, R. & Lippmaa, M. Transport properties of $\text{LaTiO}_3/\text{SrTiO}_3$ superlattices. Applied Physics Letters, **96**(19): 192111 (2010).
- [47] Paudyal, D.; Pecharsky, V. K., & Gschneidner Jr, K. A. Electronic structure, magnetic properties, and magnetostructural transformations in rare earth dialuminides. Journal of Applied Physics, **115**(17): 17E127 (2014).
- [48] Cwik, M.; Braden, M. *et. al.* Crystal and magnetic structure of LaTiO_3 : Evidence for nondegenerate t_{2g} orbitals. Physical Review B, **68**(6): 060401 (2003).

- [49] Ramay, S. M.; Mahmood, A. *et.al.* The study of electronic, magnetic, magneto-optical and thermoelectric properties of XCr_2O_4 ($X= Zn, Cd$) through modified Becke and Johnson potential scheme (mBJ). *Current Applied Physics*, **17**(8): 1038-1045 (2017).
- [50] Pandey, S.; Kaphle, G. C. & Adhikari, N. P. Electronic structure and magnetic properties of bulk elements (Fe and Pd) and ordered binary alloys (FePd and Fe_3Pd): TB-LMTO-ASA. *BIBECHANA*, **11**: 60-69(2014).
- [51] Gopal, P.; De Gennaro, R.; dos Santos Gusmao, M. S.; Al Orabi, R. A. R.; Wang, H.; Curtarolo, S.; & Nardelli, M. B. Improved electronic structure and magnetic exchange interactions in transition metal oxides. *Journal of Physics: Condensed Matter*, **29**(44): 444003(2017).
- [52] Dong, S.; Yu, R.; Yunoki, S.; Alvarez, G.; Liu, J. M., & Dagotto, E. Magnetism, conductivity, and orbital order in $(LaMnO_3)_2n/(SrMnO_3)_n$ superlattices. *Physical Review B*, **78**(20): 201102 (2008).
- [53] Zhong, Z. & Hansmann, P. Tuning the work function in transition metal oxides and their superlattices. *Physical Review B*, **93**(23): 235116 (2016).
- [54] Veit, M. J.; *et al.* "Three-dimensional character of the Fermi surface in ultrathin $LaTiO_3/SrTiO_3$ superlattices." *Physical Review B* **99**:11: 115126 (2019).
- [55] Kachhava, C. M. *Solid state physics*. McGraw-Hill Publishing Company Ltd. (1992).
- [56] Santana, J. A. & Reboredo, F. A. Electron Confinement and Magnetism of $(LaTiO_3)_1/(SrTiO_3)_5$ Superlattice: A Diffusion Quantum Monte Carlo Study. *Journal of Chemical Theory and Computation*, **16**(1): 643-650 (2019).
- [57] Wang, L.; Li, Y.; Bera, A.; Ma, C.; Jin, F.; Yuan, K. & Prellier, W. Device performance of the mott insulator $LaVO_3$ as a photovoltaic material. *Physical Review Applied*, **3**(6): 064015 (2015).
- [58] Haule, Kristjan. "Quantum Monte Carlo impurity solver for cluster dynamical mean field theory and electronic structure calculations with adjustable cluster base." *Physical Review B* **75**:15: 155113 (2007).
- [59] Pavarini, E.; Koch, E.; Vollhardt, D. & Lichtenstein, A. (Eds.). *Dmft at 25: Infinite dimensions: Lecture notes of the autumn school on correlated electron* (Vol. 4). Forschungszentrum Jülich (2014).
- [60] Van Campenhout, J. & Cover, T. Maximum entropy and conditional probability. *IEEE Transactions on Information Theory*, **27**(4): 483-489(1981).
- [61] Sevik, C. & Çağın, T. Ab initio study of thermoelectric transport properties of pure and doped quaternary compounds. *Physical Review B*, **82**(4): 045202 (2010).
- [62] Zhang, Y.; Sugo, K.; Cho, H. J. & Ohta, H. Thermoelectric phase diagram of the $SrTiO_3$ - $LaTiO_3$ solid-solution system through a metal to Mott insulator transition. *Journal of Applied Physics*, **126**(7): 075104 (2019).
- [63] Walia, S. & Kalantar-zadeh, K. Transition metal oxides–Thermoelectric properties. *Progress in Materials Science*, **58**(8): 1443-1489(2013).
- [64] Sulpizio, J. A. & Levy, J. Nanoscale phenomena in oxide superlattices. *Annual Review of Materials Research*, **44**: 117-149 (2014).
- [65] Assmann, E. & Sangiovanni, G. Oxide superlattices for efficient solar cells. *Physical review letters*, **110**(7): 078701 (2013).
- [66] Ghising, P. & Hossain, Z. Kondo effect with tunable spin–orbit interaction in $LaTiO_3/CeTiO_3/SrTiO_3$ superlattice. *Journal of Physics: Condensed Matter*.
- [67] Chen, H. A First Principles Study on Oxide Surfaces (2012).
- [68] Xue, Y. & Xu, H. Tunable magnetism in the $LaAlO_3/SrTiO_3$ superlattice: Insights from first-principles calculations. *Physica E: Low-dimensional Systems and Nanostructures*, **98**: 120-124 (2018).
- [69] Tully, J. Crisp: The center for research on interface structures and phenomena, Yale university. *Advanced Materials*, **22**(26-27): 2837 (2010).
- [70] Hirayama, M.; Miyake, T. & Imada, M. Ab initio Low-energy model of transition-metal oxide superlattice $LaAlO_3/SrTiO_3$. *Journal of the Physical Society of Japan*, **81**(8): 084708 (2012).
- [71] Gandolfi, M.; Giannetti, C. *et. al.* Emergent ultrafast phenomena in correlated oxides and superlattices. *Physica Scripta*, **92**(3): 034004 (2017).
- [72] Paudyal, D.; Pecharsky, V. K. & Gschneidner Jr, K. A. Electronic structure, magnetic properties, and magnetostructural transformations in rare earth dialuminides. *Journal of Applied Physics*, **115**(17): 17E127(2014).
- [73] Zhong Z. and Kelly, P. J. *Europhys. Lett.* **84**: 27001 (2008).
- [74] Fennie, C. J. Ferroelectrically induced weak ferromagnetism by design. *Physical review letters*, **100**(16): 167203 (2008).
- [75] Bousquet, E.; Ghosez, P. *et. al.* Improper ferroelectricity in perovskite oxide out artificial superlattices. *Nature*, **452**(7188): 732 (2008).

- [76] Brito, W. H.; Aguiar, M. C. O.; Haule, K. & Kotliar, G. Metal-insulator transition in VO_2 : A DFT+DMFT perspective. *Physical review letters*, **117**(5): 056402 (2016).
- [77] Ishida, H. & Liebsch, A. Origin of metallicity of $\text{LaTiO}_3/\text{SrTiO}_3$ superlattices. *Physical Review B*, **77**(11): 115350 (2008).
- [78] Wang, L.; Liu, Y. H. & Harcos, G. *et. al.* Split orthogonal group: A guiding principle for sign-problem-free fermionic simulations. *Physical review letters*, **115**(25): 250601 (2015).
- [79] Dine, K.; Zaoui, A. & Bouhafs, B. Fermi Surfaces of Compensated and Uncompensated Metals: GGA+U+ SO Comparative Ab Initio Study. *Journal of Superconductivity and Novel Magnetism*, **29**(8): 2195-2201(2016).
- [80] Lieb, E. H. The Hubbard model: Some rigorous results and open problems. In *Condensed Matter Physics and Exactly Soluble Models* (pp. 59-77). Springer, Berlin, Heidelberg (2004).
- [82] Araizi-Kanoutas, G. & Fatermans, J. *et. al.* Covalence transformation in isopolar $\text{LaCoO}_3/\text{LaTiO}_3$ perovskite heterostructures via interfacial engineering. *Physical Review Materials*, **4**(2): 026001(2020).
- [83] Okamoto, S.; Millis, A. J. & Spaldin, N. A. Lattice relaxation in oxide superlattices: $\text{LaTiO}_3/\text{SrTiO}_3$ superlattices. *Physical review letters*, **97**(5): 056802 (2006).
- [84] Nazir, S.; Bernal, C. & Yang, K. Modulated Two-Dimensional Charge-Carrier Density in LaTiO_3 -Layer-Doped $\text{LaAlO}_3/\text{SrTiO}_3$ Superlattice. *ACS applied materials & interfaces*, **7**(9): 5305-5311 (2015).